# Fabrication of Polyimide Shells for Use as ICF Targets

The current target-shell material for direct-drive experiments on OMEGA is a low-density hydrocarbon polymer fabricated using a low-pressure plasma polymerization process. This material meets the immediate requirements for an inertial confinement fusion (ICF) target shell: low density; smooth surfaces (outer and inner); spherical and concentric; and the capability of being fabricated with dopants at discrete radial positions in the shell wall. Future ICF experiments, especially those conducted at cryogenic temperatures, would benefit if the targets possessed additional properties: higher tensile strength; larger elastic moduli; greater room-temperature permeability; greater radiation resistance; higher thermal conductivity and lower electrical conductivity; and greater opacity at ~351 nm. These desirable properties will allow targets to be filled more rapidly with DT; be cooled faster to the DT triple point (19.8 K); survive higher temperature gradients in a cryostat; better resist the damaging effects of $\beta$-decay from tritium; and more readily accommodate augmented layering techniques such as RF-coupled joule heating. These properties will also allow decreasingly thin-walled shells to be used to contain the DT fuel; the goal is a 1-mm-diam target with a 1-$\mu$m-thick wall.

Polyimide is the only polymeric material with the potential for meeting these additional material requirements. Scientists at Lawrence Livermore National Laboratory were the first to suggest polyimide[1] targets for the National Ignition Facility (NIF). If targets could be fabricated with the same strength as commercial polyimide films, then cryogenic targets could be filled and transported at room temperature and frozen only immediately prior to the experiment. (The requirements for a NIF target are 2.2-mm outer diameter, 160-$\mu$m walls, and a DT room-temperature fill pressure of ~360 atm.) These simplifications would substantially reduce the complexity and cost of implementing indirect-drive cryogenic targets on the NIF.

Postulating and theoretically validating polyimide shells as a viable ICF target design were necessary first steps. Fabricating polyimide shells to experimentally quantify the material properties is the next phase. No polyimide shells have been made until now because the available polyimide fabrication techniques could not be adapted to current target-fabrication technology. Two recent developments, one in the area of ICF target-fabrication methods and the other in the area of polyimide fabrication for microelectronics applications, have provided a method for fabricating polyimide targets: (1) the development of a decomposable polymer mandrel for making the present ICF targets and (2) the development of a technique for vapor-depositing polyimide films. This study employs the combination of these two techniques to produce polyimide shells and presents property data of the resultant material.

## Background

### 1. Preparation of Solution-Cast Polyimide Films

Polyimides are usually produced in a two-step synthesis:[2] First, an aromatic diamine (e.g., ODA) is dissolved in a polar solvent such as dimethylformamide. An aromatic dianhydride (e.g., PMDA) is then added to the solution to form the soluble polyamic acid. The polyamic acid solution is spun-cast onto flat substrates and then thermally cured at 300°C to form the polyimide. The chemical structures are shown in Fig. 71.14. There is no straightforward way this technique can be adapted to make ICF targets using established microencapsulation methods. Furthermore, there are technical issues with this technique that may render the material unsuitable as a target shell material: polyamic acids are hydrolytically unstable; solvents may remain in the film; adverse interaction may occur between the solvent and the substrate (i.e., mandrel); and the viscosity of the polymer solution may make it difficult to control the thickness and uniformity of the shell wall.

### 2. Preparation of Vapor-Deposited Polyimide Films

The vapor-deposition-polymerization[3,4] (VDP) technique of making polyimide film was developed to provide a solvent-less method of depositing conformal dielectric coatings. The process involved three steps: (1) dianhydride and diamine monomers were sublimed under high vacuum, (2) the vapor phase monomers reacted to form polyamic acid on the surface of the substrate, and (3) the polyamic acid was thermally cured at 300°C to form polyimide. The advantages of this pro-
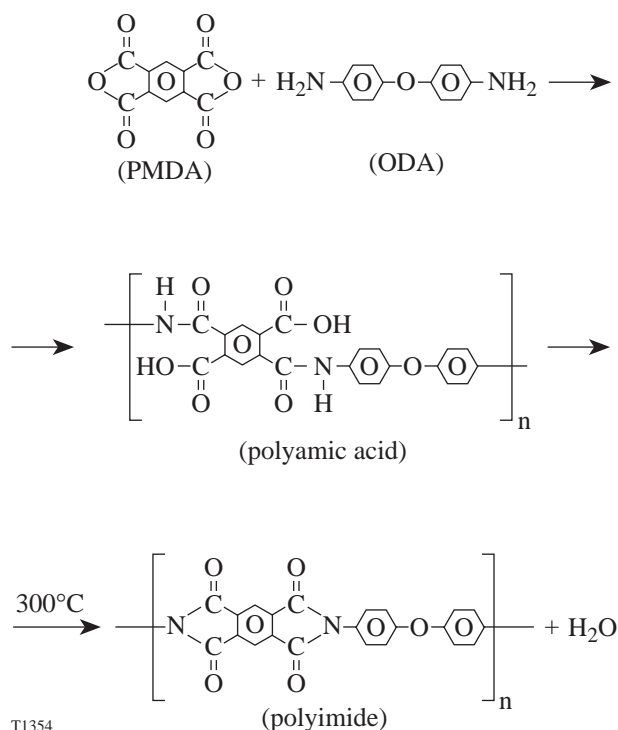
Figure 71.14
Formation of polyimide from pyromellitic dianhydride (PMDA) and oxydianiline (ODA) precursors.

cessing technique are the lack of detrimental solvent effects (i.e., vacuoles) and the uniformity of the film thickness. This technique was used in this study to make OMEGA-size ICF targets by depositing the film on spherical depolymerizable mandrels.

3. Fabrication of Targets Using Depolymerizable Mandrels
The depolymerizable mandrel technique was recently developed to fabricate plastic ICF targets.[5] The mandrels were either solid beads or hollow shells made from poly($\alpha$-methylstyrene) (PAMS) that were overcoated with plasma polymer using the traditional low-pressure glow discharge polymerization process.[6] Heating the overcoated mandrel to 300°C decomposes the mandrel into its individual monomer units that permeate through the shell wall. The importance of the PAMS formulation is that it undergoes complete depolymerization into gaseous monomers at a relatively low temperature (160°C–300°C), where the plasma polymer outer shell is thermally stable.

Currently, the PAMS mandrels are thin-walled (~20-μm) shells (0.70- to 0.95-mm diam) fabricated by the micro-encapsulation method.[7] (This method was initially developed to

make polystyrene shells for ICF experiments but is better suited for making mandrels.) A critical requirement of the mandrel, which has been demonstrated,[8] is a smooth, spherical surface.

4. Comparison of Target-Material Relevant Properties
Table 71.I compares the relevant properties of the current target-shell material against the properties of polyimides fabricated using both solution-cast and vapor-phase-deposition techniques.

There are many formulations of solution-cast polyimide films, and the material properties are well defined. The values listed here are the optimal values reported for two types of commercially available polyimide: Upilex-S and Kapton. The values listed for vapor-deposited polyimide films are from the literature. However, these values possess greater uncertainties and are likely to be more process dependent. The strength and modulus values listed for ICF shells are the best estimates derived from a limited set of burst and buckle tests of 1-mm-diam shells.

**Fabrication and Characterization**
1. Materials
Pyromellitic dianhydride (PMDA) (1,2,4,5-benzenetetra-carboxylic dianhydride; 97% purity) and 4,4'-oxydianiline (ODA) (99+% purity; zone refined) were received from Aldrich Chemical and used without further purification. Poly($\alpha$-methylstyrene) mandrels were received from General Atomics (850- to 950-μm inner diam; ~20-μm wall thickness; MW 400,000) or fabricated in-house (700- to 950-μm inner diam; ~10-μm wall thickness; MW 97,500).

2. Deposition Equipment
The deposition system consists of a vacuum chamber, mechanical pump, and two identical evaporation sources, one each for PMDA and ODA (Fig. 71.15). The chamber was a stainless steel cube with an adapting tee (6-liter internal volume) and three glass viewports. The system was pumped with a mechanical pump (Alcatel model 2010) through two liquid nitrogen foreline traps and achieved a base pressure of 1 mTorr. Each evaporation source was a copper cylinder containing a 0.3-cm-outer-diam × 5-cm cartridge heater (Watlow Firerod; 50 W max) and a K-type thermocouple. The temperature was maintained within ±1.0°C of the set point using a proportional-integral-derivative controller (Omega CN9000).

Each evaporation source contained ~50 mg of monomer, which was sufficient material for an 8-h process cycle. The

Table 71.I: A comparison of available relevant material properties of existing ICF shells and two types of polyimide.

| | Current ICF Plasma Polymer Shell | Vapor-Deposited Polyimide Film | Solution-Cast Polyimide Film |
|---|---|---|---|
| Ultimate tensile strength (MPa) at 300 K at cryogenic temperatures | $75\pm15$[a] $160\pm12$ at 40 K[b] | 120–170[c,d] – | 420[e] 500 at 77 K[e] |
| Elastic modulus (GPa) at 300 K at cryogenic temperatures | 3.1[a] 9.7 at 15 K[*] | 2.3 –4.0[c,d] – | 9.3[e] 12 at 77 K[e] |
| Density (g/cm$^3$) | 1.039 | 1.39[d] | 1.42[f] |
| Coefficient of thermal conductivity (W/m•K) | 0.04 at 20 K[**] | – – | 0.82 at 293 K[g] 0.08 at 20 K[g] |
| Dielectric constant | 2.5 (at 1 MHz)[**] | 2.91 (at 1 MHz)[c] | 3.4 (at 1 GHz)[f] |
| Radiation resistance (electron) (dose required to reduce the maximum elongation by 50%) | – | – | $6 \times 10^7$ Gy[f] ($1 \times 10^{14}$ Ci·s) |
| Permeability at 300 K (mol•m/m$^2$•P a•s) | $6.5 \times 10^{-15}$ (for D$_2$)[a] | $1 \times 10^{-19}$ (for O$_2$)[*] | $2.9 \times 10^{-15}$ (for H$_2$)[h] |

[*]  data for a polyamide film.
[**]  data for a polystyrene film.
[a]  R. Gram, UR/LLE (private communication).
[b]  N. Alexander, General Atomics (private communication).
[c]  Ref. 3.
[d]  M. Iijima, Y. Takahashi, High Perform. Polym. **5**, 229 (1993).
[e]  H. Yamaoka, K. Miyata, O. Yano, Cryogenics **35**, 787 (1995).
[f]  DuPont Technical Bulletin.  Product information for Kapton Type-H film.
[g]  H. Yokoyama, Cryogenics **35**, 799 (1995).
[h]  Ref. 15.

optimal processing conditions that yielded a uniform distribution of each monomer in near-stoichiometric proportions are listed in Table 71.II. The partial vapor pressure of PMDA and ODA at these conditions was 0.35 and 0.15 mbar[9] (0.26 and 0.11 Torr), respectively.

The preferred experimental configuration for making particulate-free coatings is to suspend the substrate upside down in the vacuum chamber with the evaporation sources directly beneath the substrate. This configuration cannot be used with the existing bounce-coating method for coating shells, so the evaporation sources were built to direct the monomer flow downward onto the substrate. The substrates were either flat witness plates (NaCl and silicon wafers) mounted on a thermally isolated support or spherical mandrels placed in a bounce pan. The bounce pan consisted of a 2-cm curved dish with a piezoelectric element attached to the base. A 5-V, 3-kHz signal applied to the piezo-material maintained the shells in a gentle, random motion during the deposition process. Unlike previous techniques used to coat shells (e.g., plasma parylene
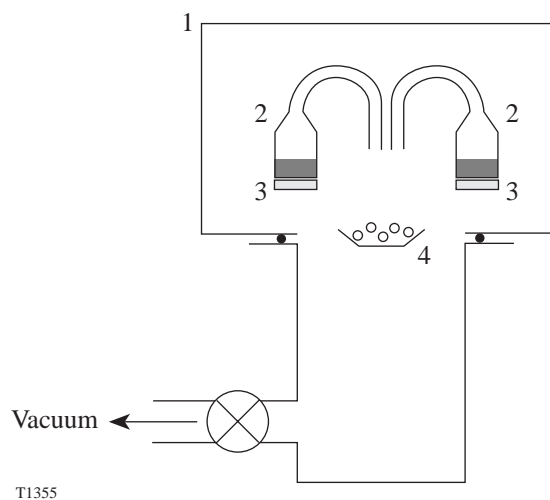


T1355

Figure 71.15
Schematic of the deposition chamber: (1) vacuum chamber, (2) deposition source, (3) heater, and (4) bounce pan containing shells.

Table 71.II:  Processing conditions used to deposit polyamic acid films from PMDA–ODA monomers.

| PMDA temperature | 160°C |
|---|---|
| ODA temperature | 140°C |
| System pressure | 1 to $30 \times 10^{-3}$ Torr |
| Separation between evaporation sources and substrate | 5 cm |
| Diameter of substrate that received a uniform coating | 3 cm |
| Coating rate on shells | 0.8–1.0 $\mu$m/h |
| Coating rate on flat substrates | ~3 $\mu$m/h |

and plasma polymer), the VDP-polyimide technique does not require a plasma to initiate or accelerate the polymerization process. However, the plasma had an essential serendipitous benefit of preventing shells from sticking together by overcoming the static charge that developed as targets rubbed against each other. (Shells bouncing in the sheath of the RF plasma developed a similar potential that swamped the friction-induced static charge and caused the shells to mutually repel.)

The experimental equipment was modified to add a mechanism to overcome the induced static charge. First, a copper electrode was added inside the vacuum chamber to ignite an argon plasma (glow discharge). The pressure was increased from 1 to ~30 mTorr (using argon), and the plasma was maintained for the minimum period necessary to dislodge the shells from the pan (~15 s every 15 min). An alternative method of dissipating the static charge used a thermionic electron source directed at the pan. A tungsten filament was positioned ~1 cm from the pan, and a constant current (6 mA) was maintained through the filament. The resulting flood of electrons negatively biased the shells and prevented them from sticking together. This process was independent of pressure, which permitted the base pressure of 1 mTorr to be maintained during deposition. Both techniques successfully prevented shells from sticking to themselves or the pan during the >6-h processes, and shells made by both techniques were evaluated in subsequent tests.

### 3. Heating Cycle

A programmable vacuum furnace (Ney Centurion VPM) was used to thermally convert (i.e., imidize) the polyamic acid shells to polyimide, and to decompose the inner PAMS mandrel. The furnace's cylindrical heated zone was 10-cm diam × 6.3-cm high, and the progress of the depolymerization process was monitored through a glass viewport. The heating cycle was performed in a static air environment. The heating rate was controlled with an accuracy of ±0.1°C/min.

Each shell was placed in a separate glass tube in the furnace to protect it from fratricidal impact should any shell burst during curing. The optimum heating cycle (Fig. 71.16) required the temperature to be raised from 25°C to 140°C at 2.0°C/min, with a 2-h dwell, then raised to 150°C (5-h dwell), 180°C (12-h dwell), 220°C (12-h dwell), and 300°C (24-h dwell), at a rate of 0.1°C/min. After the final heating stage the furnace cooled to room temperature at ~0.5°C/min.
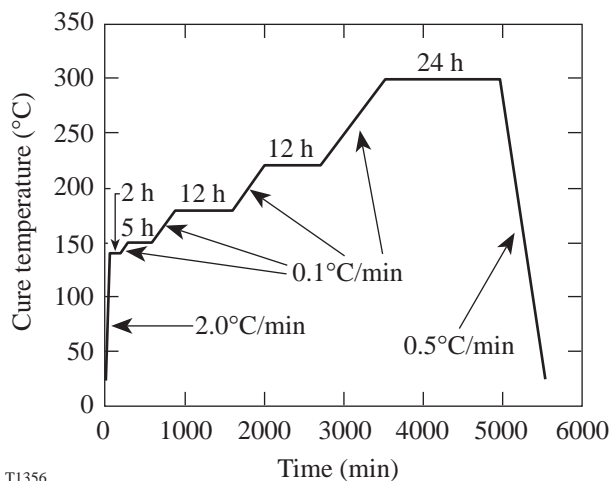


T1356

Figure 71.16
Curing cycle used to imidize the polyamic acid and depolymerize the PAMS mandrel.

### 4. Chemical Analysis—FTIR Measurements

The monomer precursors were co-deposited onto NaCl substrates for Fourier transform infrared (FTIR) characterization. FTIR spectra were taken on the as-deposited, partially cured, and fully cured films, as shown in Fig. 71.17. The spectrum of the as-deposited film showed absorption peaks at ~1850 and 1780 cm$^{-1}$ due to the carboxylic acid anhydride and peaks at ~1650 and 1550 cm$^{-1}$ due to amide couplings {[C=O(CONH)] and (C-NH), respectively}. These spectra indicated that the as-deposited film consisted of nonreacted
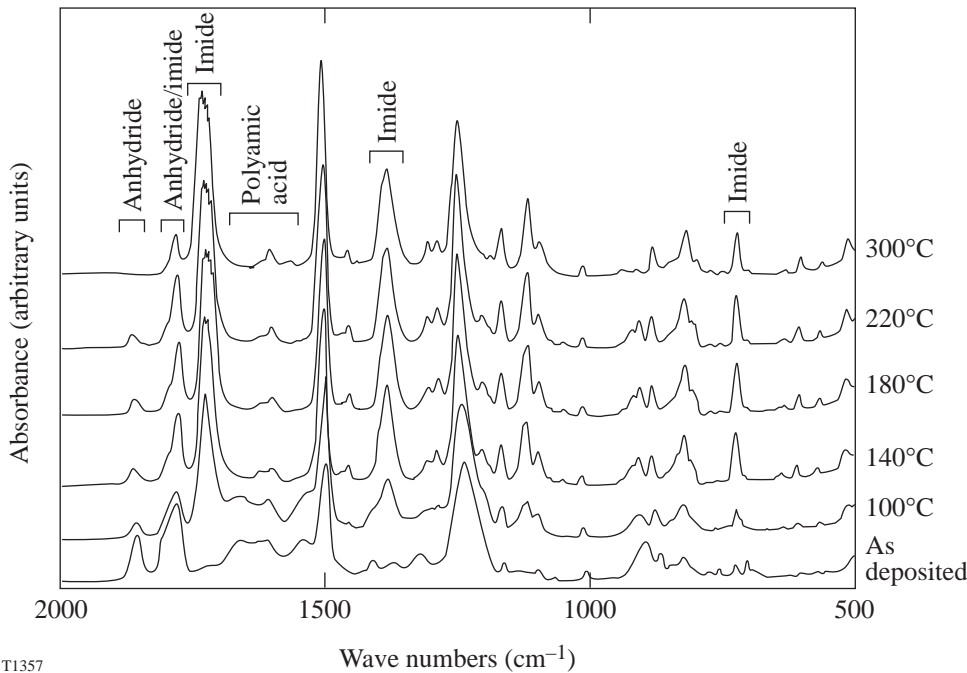
Figure 71.17
FTIR spectra of the as-deposited, partially cured, and fully cured PMDA-ODA/ polyamic acid/polyimide film. The characteristic polyimide peaks appear as the material cures.

T1357

monomers and polyamic acid. After curing at 300°C for 60 min, the imide absorption peaks were dominant: $1780 \, cm^{-1}$ (C=O asym. stretch), $1720 \, cm^{-1}$ (C=O sym. stretch), $1380 \, cm^{-1}$ (C-N stretch), and $725 \, cm^{-1}$ (C=O bend), and the amide coupling and carboxylic acid anhydride absorption peaks had disappeared. These spectra agree with similar results published in the literature.[3,10] [The formal name for this polymer is poly(N,N'-bis(phenoxyphenyl) pyromellitimide) and is commonly known as PMDA–ODA polyimide. A solution-cast version is sold under the trade name Kapton®.]

5. Shell Dimensions

The outside diameter of the shells was measured to an accuracy of $\pm 1 \, \mu$m using a Nikon Optiphot optical microscope equipped with a HMOS Micro-Measure digital scaler. The wall thickness was determined from SEM micrographs of cross sections through the shell with an accuracy of $\pm 0.3 \, \mu$m. (The targets were too opaque to use interferometry to measure the wall thickness.)

The sphericity was determined by measuring the outer diameter along a single axis and then repeating the process for additional axes. The sphericity $s$ of a shell was defined as $s = \left[ 1 - \left( D_{max} - D_{avg} \right) / D_{avg} \right] \times 100\%$, where $D_{max}$ is the maximum diameter and $D_{avg}$ is the average diameter from 12 measurements. The sphericity of the polyimide shells was >99%, a value consistent with plasma polymer shells fabricated by the decomposable mandrel technique.

Imidizing the polyamic acid and depolymerizing the mandrel caused the resulting polyimide shell to be smaller and thinner than the original polyamic acid shell. The polyimide shell's outer diameter was 1% to 2% smaller than the original diameter. The polyimide wall was 20% to 30% thinner than the wall of the polyamic acid shell. The range of dimensions of all the polyimide shells is listed in Table 71.III.

Table 71.III: Typical dimensions of polyimide shells successfully fabricated in this study.

| | |
|---|---|
| Inner diameter | 700 to 950 $\mu$m |
| Wall thickness | 4 to 13 $\mu$m |
| Sphericity | > 99% |
| Shrinkage: wall outer diameter | 20%– 30% 1%–2% |
| Density | 1.21 to 1.40 g/cm³ |

6. Elemental Composition—RBS Measurements

The elemental composition of the fully imidized polyimide film was measured using Rutherford backscattering (RBS) analysis. The RBS technique has the advantage of providing absolute quantitative data without calibrating against NIST–traceable standards. Also, the technique can be used to study a single shell (probe size ~5-$\mu$m-diam circle) and can provide depth-resolved compositional data.

The data were acquired using the Dynamitron at the Nuclear Laboratory at the State University of New York at Albany. The recoil data were fitted using the RUMP program. A 2-MeV He beam was used to acquire the backscattered signal. The total charge from the beam was kept below 6 $\mu$C to prevent the beam from heating the film and changing the elemental composition.

The measured elemental composition of one of the polyimide films was 50 at.% carbon; 37 at.% hydrogen; 9 at.% oxygen; and 4 at.% nitrogen. The uncertainty was ~20%. The theoretical composition of a PMDA-ODA polyimide is 56 at.% carbon; 26 at.% hydrogen; 13 at.% oxygen; and 5 at.% nitrogen.

### 7. Burst and Buckle Pressure Measurements

The equipment consisted of a pressure cell with opposing windows, a microscope, a CCD camera, and a pressure transducer (Omega PX621) with an accuracy of ±1 psi. The shells were viewed through a microscope with transmitted light. The shell's image, the gas pressure in the cell, and the lapsed time were all recorded on videotape.

To burst (or buckle) a shell, the pressure in the chamber was lowered (or raised) at a faster rate than the rate the internal shell pressure changed due to permeation through the shell wall. Typical pressure-rate changes ranged from 0.01 atm/s to 3.5 atm/s for buckle tests and up to 50 atm/s for burst tests. After the shell failed, the video tape was reviewed frame-by-frame to determine the exact rupture pressure. If the permeation time constant of the shell was known, the pressure difference across the shell wall at the point of failure could be accurately calculated, and the strength measurement was corrected for this change.

### 8. Permeability and Time Constant Measurements

a. For shells. The permeability of a shell was measured[11] by permeating gas into the shell and then transferring it into a (pre-baked) chamber of known volume (2.4 cm$^3$). The pressure rise in the chamber was monitored as a function of time, and the data were fitted with the expected exponential function. A correction term was added to this function to account for outgassing from the chamber walls (~4 × 10$^{-11}$ Torr•$\ell$/cm$^2$•s). The equation gives the shell's permeation time constant (for the specific gas) and the total quantity of gas in the shell at the time the pressure measurement began. The technique allowed permeation time constants as short as 1 min and as long as 50 h to be measured with an accuracy greater than 95%.

The permeation time constant $\tau$ was determined from the plot of pressure rise versus time. The material permeability coefficient $K_p$ was determined using the permeation time constant of a thin spherical container, $\tau^{-1} = (K_p A R_g T)/wV$, where $A$ is the shell's mean surface area, $R_g$ is the ideal gas constant, $T$ is the absolute temperature, $w$ is the shell wall thickness, and $V$ is the shell volume. For a thin-walled spherical shell this simplifies to $K_p = w\langle r\rangle/3\tau R_g T$, where $\langle r\rangle$ is the average shell radius.

b. For flat films. The equipment and test method were based upon the ASTM procedure, which estimates the steady-state rate of transmission of a gas through plastics in the form of a film, sheeting, laminates, and plastic-coated papers or fabrics.[12] A flat, freestanding polyimide film was mounted in a gas transmission cell to form a sealed semibarrier between two chambers. One chamber contained the test gas at a specific high pressure, and the other chamber, initially evacuated, received the permeating gas. The rate of gas transmission through the polyimide film was determined from the measured pressure rise in the downstream chamber. The permeability of 1-cm-diam, 14.7-$\mu$m-thick polyimide films was then measured using deuterium and nitrogen. Equipment accuracy was tested by comparing the measured permeability of commercial polyimide films (Kapton and Upilex-R) against the reported values; the agreement was within 50%.

### 9. Roughness Measurements

Surfaces of the shells and flat films along with cross sections of the shell walls were inspected using a scanning electron microscope (Cambridge Instruments, model S200). The micrographs provided a qualitative measurement of the surfaces' morphology and roughness. Quantitative measurements were obtained using atomic force microscopy (AFM): flat polyimide films on silicon witness plates were analyzed using a Nanoscope III instrument (Digital Instruments); and shells were analyzed using an AFM modified to measure 1-mm-diam shells. The latter technique, performed by General Atomics, measured the roughness along great arcs of a circle around a sphere. Generally, the flat films were very smooth and the spheres were rough (data discussed in detail later).

### 10. Mechanical Behavior—Stress Measurements

The residual stress that develops in the polymer during the imidizing cycle must be known so that the heating cycle can be optimized to minimize the induced stress. Shells that crack during curing behave this way because of the rate and magnitude at which the stress develops in the shell wall. In this

process, the change in the residual stress was expected to be significant; imidization involves an appreciable mass loss and a substantial change in the structure and morphology of the polymer as the polyamic acid is converted into an increasingly high-molecular-weight polyimide.

Thin polyamic acid films were deposited on high-aspect-ratio silicon (100) substrates (1 cm × 0.1 cm × 0.25 mm thick). The curvature of the substrate was measured prior to, and following, deposition using a profilometer (Rank Taylor Hobson Talysurf). The measured change in the radius of curvature ($\Delta R$) due to the polymer film yielded the total stress ($\sigma_{\text{total}}$) in the film:[13]

$$\sigma_{\text{total}} = \left[E_s / 6(1 - v_s)\right]\left[t_{\text{substrate}}^2 / t_{\text{film}}\right]\left[\Delta R^{-1}\right],$$

where $E_s$ is the elastic modulus of the silicon substrate, $v_s$ is the Poisson ratio, and $t$ is the thickness of the film/substrate. The total stress was the sum of the intrinsic stress and the induced thermal stress (due to the thermal coefficient mismatch between the silicon substrate and the deposited film) that arises because the film was imidized at an elevated temperature and the stress was measured at room temperature. The thermal stress ($\sigma_{\text{thermal}}$) is given by

$$\sigma_{\text{thermal}} = \left[E_f / (1 - v_f)\right]\left[\alpha_{\text{silicon}} - \alpha_{\text{polyimide}}\right]\Delta T,$$

where $E_f$ and $v_f$ are the elastic modulus and Poisson ratio of the polyimide film, respectively, $\alpha$ is the coefficient of thermal expansion for the silicon/polyimide, and $\Delta T$ is the difference between the cure and measurement temperatures. Subtracting the thermal stress determined the intrinsic component of the residual stress. These data are discussed later.

**Discussion**

1. Optimizing the Processing Conditions

The first task was to define the operating parameters required to deposit thin films of polyamic acid with a stoichiometric balance of PMDA and ODA monomers. Optical macrographs and FTIR spectra of the films deposited on flat NaCl witness substrates showed the importance of (1) positioning the substrate relative to the PMDA and ODA evaporation sources and (2) the temperature of the evaporation sources. The film deposited at the center of the substrate experienced an equivalent flux of each monomer and was opaque. FTIR spectra of this region identified polyamic acid as the primary

component. The perimeter of the substrate possessed a film that was thinner and more transparent than the center and contained excess PMDA or ODA, depending upon the substrate's position relative to the evaporation sources. Rotating the substrate during deposition improved the uniformity of the film's thickness and composition. These experiments defined the optimal distance between the evaporation sources and the substrate, the required temperature of the evaporation sources, the maximum diameter of the substrate that was uniformly coated with polyamic acid, and the resultant deposition rate (see Table 71.II). Examples of the FTIR data for this analysis are shown in Fig. 71.18 and compared to spectra reported in the literature.[3] Here, the relation between the film's composition and the evaporation source temperature was demonstrated. When the source temperatures for PMDA and ODA were 160°C and 120°C, respectively, excess PMDA was present in the film, and the characteristic dianhydride peaks at 1780, 925, 905, and 720 cm$^{-1}$ were proportionally greater than the peaks attributed to ODA. Raising the ODA temperature to
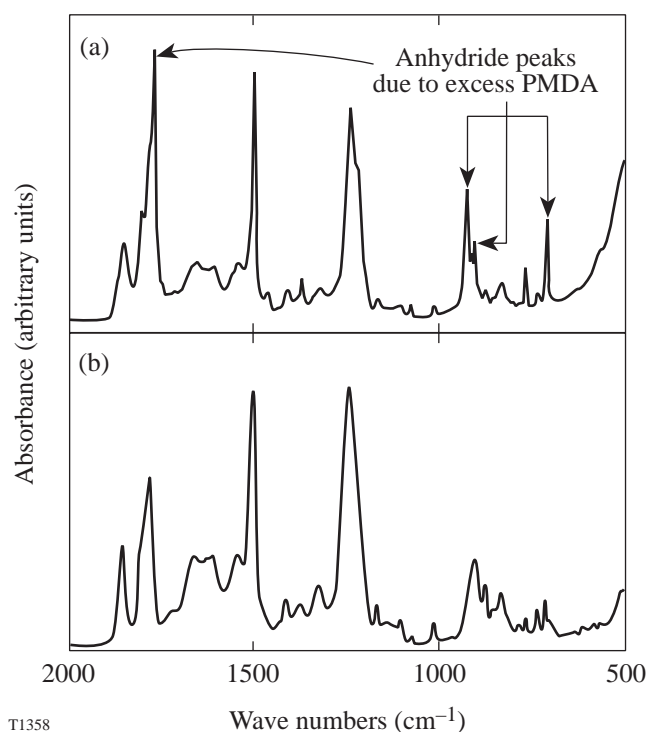


Figure 71.18
FTIR spectra of the as-deposited films made with varying ODA deposition temperatures: (a) $T_{\text{ODA}} = 122°C$, $T_{\text{PMDA}} = 160°C$; (b) $T_{\text{ODA}} = 140°C$, $T_{\text{PMDA}} = 160°C$. Spectrum (b) is identical to the polyamic acid spectrum as reported in the literature. Spectrum (a) shows anhydride peaks due to excess PMDA.

130°C provided an observed improvement, but the best results (based upon comparisons with the literature) were obtained with the source temperatures of 160°C and 140°C for PMDA and ODA, respectively. The spectrum shown in Fig. 71.18(b) is identical to that reported in the literature as a 1:1 molar ratio polyamic acid film.[3]

The next phase was to define the thermal cycle required to convert the polyamic acid into the polyimide. Typically, VDP polyamic acid films were heated to 175°C for 30 min, then to 300°C for 30 min. The cycle used for the current films included a slower ramp and was interrupted at 100, 140, 180, and 220°C to monitor the changing chemical and mechanical composition of the film. FTIR spectra of the polyamic-acid–coated NaCl substrate were acquired, and the change in curvature of the coated Si substrate was measured.

Conversion of polyamic acid into polyimide was evident at the first inspection at 100°C. Two characteristic absorption peaks were present: the C-N stretch frequency at 1380 cm$^{-1}$ and the C=O asymmetric stretch at 1720 cm$^{-1}$ (Fig. 71.17). This observation is consistent with reports that state VDP polyamic acid films begin imidization at lower temperatures than do solution-cast films.[14] As the heating cycle progressed, the imide peaks became more prominent and the polyamic acid absorption peaks (at 1650 to 1550 cm$^{-1}$) diminished. Anhydride peaks (1850 cm$^{-1}$) were still visible after heating to 220°C but disappeared after the final curing stage at 300°C. The changes in the stress that accompanied these chemical changes are described later.

The heating cycle used above was inadequate for imidizing polyamic-acid–coated PAMS shells; the simultaneous depolymerization of the PAMS mandrel overpressurized the shells, causing them to burst. A considerably slower heating ramp (see Fig. 71.16), with longer dwells at critical temperatures,

was required to balance the rate at which PAMS decomposed with the rate at which $\alpha$-methylstyrene permeated through the polyamic acid/polyimide/PAMS shell wall. This heating cycle was determined empirically since the mechanical and permeability properties of the wall could not be predicted. Several events complicated the process because they occurred simultaneously: excess monomer was subliming; PAMS was depolymerizing; the polyamic acid was reacting to form the polyimide; the softening PAMS was slumping, and the weight of the viscous material was adding a nonuniform strain to the shell wall; and the shell wall was resisting an increasing burst-pressure as the $\alpha$-methylstyrene partial pressure increased with increasing temperature. Identifying a successful heating cycle is the most important component of making thin-walled, high-aspect-ratio polyimide shells. Currently the thinnest shells successfully fabricated have 4-$\mu$m walls and 700- to 950-$\mu$m inner diameters.

### 2. Morphology of the Polyimide Material

Polyimide films (3- to 15-$\mu$m thickness) deposited on flat substrates were evaluated using optical, electron, and atomic-force microscopy and were observed to be very smooth. The rms roughness was 0.81 nm with most of the power attributed to features with a wavelength between 1 and 0.1 $\mu$m (Fig. 71.19). These results indicate that the deposition and imidizing process provided a material with a smooth surface that is acceptable for use in ICF experiments.

In contrast to the flat film, the shells possess substantial roughness. The rms roughness of a polyamic-acid shell deposited using plasma assistance was ~800 nm. This quantified roughness was consistent with SEM micrographs that showed a nodular surface with a high density of nodes 1 to 5 $\mu$m in diameter [Fig. 71.20(a)]. This roughness may be attributed to either the special processing conditions required to coat shells (the plasma- or thermionic-assisted technique) or a prob-

Total power:      0.652 nm
Equivalent rms:   0.808 nm



T1359

Power (nm$^4$) vs Wavelength ($\mu$m/cycle)
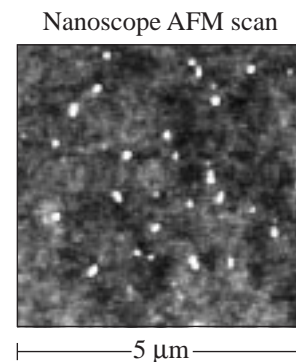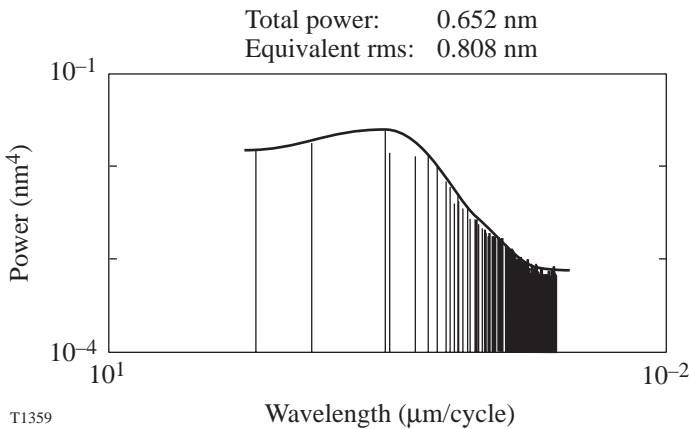


Nanoscope AFM scan

|— 5 $\mu$m —|

Figure 71.19
Power spectrum of a flat polyimide film. The rms roughness is 0.81 nm.

lem specific to forming a rigid polyimide structure in a spherical geometry.

One reason that shells possess a greater roughness than flat films is the high background pressure (20 to 30 mTorr) required by the plasma-assisted technique. A high pressure causes reacting monomers to experience thermalizing gas phase collisions before they reach the shell's surface. This reduces the mobility of the adsorbed atoms (adatoms), which prevents the nascent layer from fully relaxing before the subsequent atomic layer arrives at the surface and freezes the current distribution of adatoms in place. This loss of surface diffusivity generates nodular features with sizes inversely proportional to the adatom diffusion distance. These effects on the magnitude and frequency of the nodes are compounded by statistical fluctuations in the vapor flux, and the amplitude of the roughness grows with increasing film thickness, due to self-shadowing effects.

Polyimide shells made by the plasma-assisted method were rougher and more nodular than the shells made by the thermionic emission method. Examination of the cross sections of fractured shells deposited with plasma assistance showed that the nodular morphology and internodular porosity extend through the wall to the inner surface (Fig. 71.20), while shells deposited with thermionic assistance possessed denser walls with no visible porosity and a smooth inner surface (Fig. 71.21). Despite the improved smoothness achieved at lower processing pressures, the smoothness of the shells deposited using thermionic assistance did not qualitatively approach the smooth-
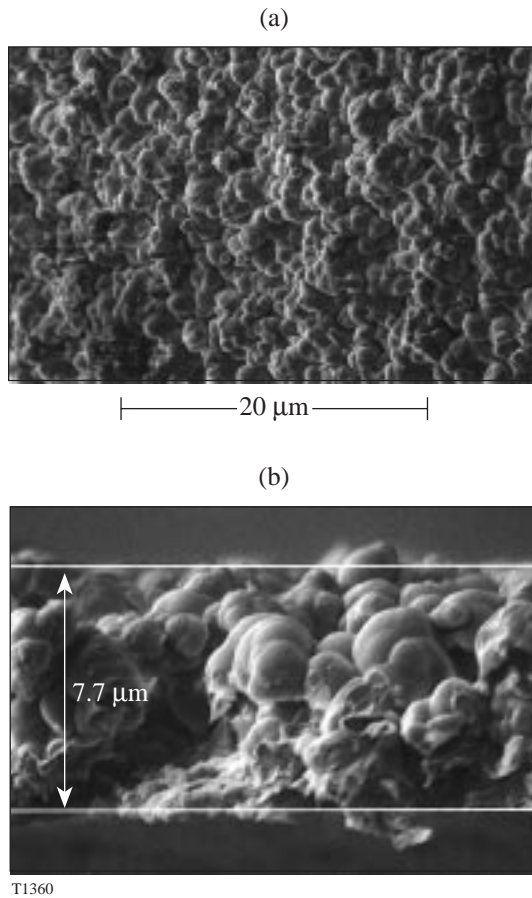
(a)



(b)



T1360

Figure 71.20
Outer surface (a) and cross section through the wall (b) of a polyimide shell made in the presence of a plasma. The nodular structure is seen through the shell wall.
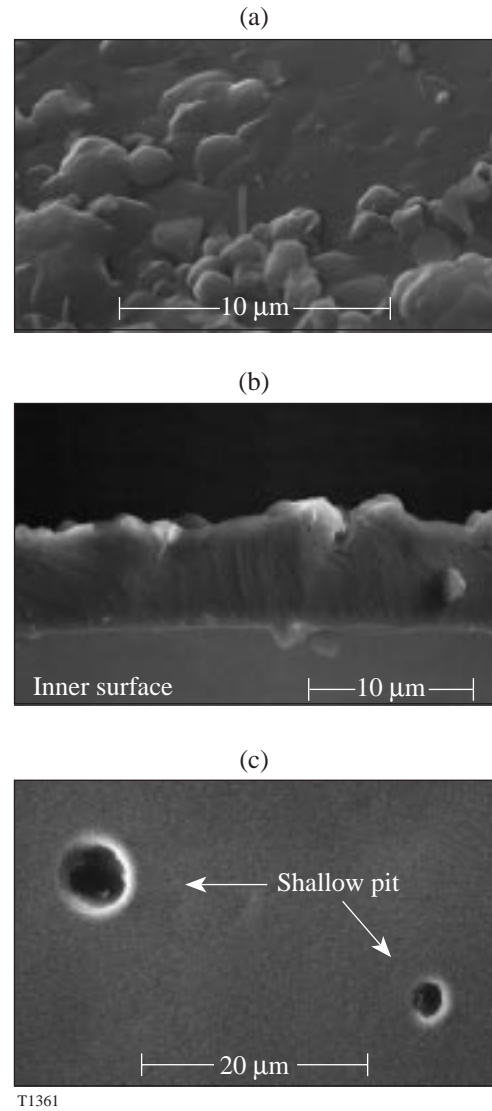
(a)



(b)



(c)



T1361

Figure 71.21
Outer surface (a), cross section through the wall (b), and inner surface (c) of a polyimide shell made in the presence of thermionic emission. The wall appears to be fully dense. The indentations on the inner surface are imprints from imperfections and debris on the PAMS mandrel.

ness of the flat films. (A quantitative comparison remains to be performed.) These observations suggest that the increased pressure contributes to, but is not solely responsible for, the shell's roughness. The only remaining differences between the processing conditions used to make flat films and spheres are the bouncing motion, spherical geometry, and substrate material of the shells, from which we conclude that one or all of these effects contribute to the observed roughness.

The inner surface of the shells deposited by thermionic emission appeared similar to the surface of plasma polymer shells currently made using the PAMS mandrel. Shallow domes (~1- to 5-$\mu$m diameter and <10 $\mu$m deep) were sparsely distributed over the inner surface [Fig. 71.21(c)]. These features are replicates of the underlying mandrel imprinted into the overcoated polyimide as a consequence of the highly conformal mapping capability of the deposition process.

3. Material Property: Permeability

The rate at which hydrogen isotopes permeate through the polyimide material is a major factor that will determine the viability of vapor-deposited polyimide films as target shell material. A high room-temperature permeation rate will allow targets to be rapidly filled to the designated pressure (maximum is 1500 atm) for cryogenic ICF experiments. A slow room-temperature permeation rate will require that the targets be filled at elevated temperatures (200°C max); otherwise the material cannot be used. It is necessary that the material be impermeable below 26 K and desirable, although unlikely, that the material be permeable above ~50 K. This latter capability will prevent a pressure differential from developing across the shell wall during the cooling cycle (due to temperature gradients in the permeation vessel).

The permeation time constant $\tau$ of deuterium for a PAMS shell at 298 K was $\tau = 1.2$ to 3.9 min ($\tau$ depends on the shell dimensions). The permeation time constant for the PAMS shells with a polyamic acid coating was $\tau = 1.12$ h. (The polyimide shells discussed here were made using the thermionic emission technique.) After the polyamic acid was imidized and the mandrel removed, the permeation time constant could not be measured. There was insufficient gas in the target to obtain a pressure reading on the apparatus; the time constant was either less than ~45 s or greater than ~50 h. The results were similar when nitrogen—a less permeable gas—was used (a time constant could not be measured with the current equipment). Unfortunately, literature values could not clarify whether the time constant was short or long: permeation rates obtained from the literature for solution-cast polyimide films

with a similar composition indicate a short time constant for hydrogen,[15] ~2.4 min, while the limited data available for vapor-deposited films suggest a very long time constant.[16]

The permeability of the shell material and underlying mandrel was measured after curing to increasingly higher temperatures of the imidizing cycle to determine at which point in the cycle the shell became more, or less, permeable. (The results are listed in Table 71.IV.) (These data are also a measure of the changing composition and structure of the shell.) The permeability of the PAMS mandrel was high ($K_p = 4.7 \times 10^{-15}$ mol•m/m$^2$•Pa•s), which yields $\tau = 1.2$ min. The permeability of the polyamic-acid–coated mandrel (6.4 $\mu$m of polyamic acid) was considerably smaller ($K_p = 0.074 \times 10^{-15}$ mol•m/m$^2$•Pa•s), which yields $\tau = 74$ min. Heating the shell to 100°C for 1.5 h decreased $\tau$ to 17 min. Further heating to 120, 140, and 150°C lowered $\tau$ to 8 to 10 min. After the 165°C cure stage, the time constant could not be measured. These data indicated the shell was becoming more permeable as imidization progressed, but more positive evidence was necessary to determine whether or not the fully imidized shell was permeable.

Table 71.IV: Permeation data for polyamic acid/polyimide shells (D$_2$ at 298 K).

| Curing Condition | $\tau$ (min) | $K_p \times 10^{17}$ (mol•m/m$^2$•Pa•s) |
|---|---|---|
| PAMS mandrel | 1.18 | 470 |
| Polyamic acid + PAMS mandrel: as-deposited | 74.4 | 7.4 |
| After 100°C at 1.5 h | 16.9 | 32 |
| After 120°C at 1.5 h | 8.54 | 64 |
| After 140°C at 3 h | 10.8 | 51 |
| After 150°C at 5 h | 8.52 | 64 |

Since critical permeation data were unobtainable for polyimide shells, a more sensitive technique using flat, vapor-deposited polyimide films was tested to obtain the values. (The results are listed in Table 71.V.) The deuterium permeability was $2.0 \times 10^{-14}$ mol•m/m$^2$•Pa•s at 298 K, and the nitrogen permeability was $8.0 \times 10^{-15}$ mol•m/m$^2$•Pa•s at 298 K. While we cannot exclude the possibility that the rapid permeation may be due to interconnected pores or pinholes in the film, no pinholes have been observed (using both AFM and SEM scans) and the size and density of any porosity are unknown. These permeability values were used to calculate time constants for typical OMEGA-size shells (Table 71.V). The time constant

Table 71.V:  Measured permeability of different shell materials used to calculate time constants for an OMEGA-size shell.

| | Permeability at 25°C (mol•m/m$^2$•Pa•s) | | Time constant for 1-mm-outer-diam, 5-$\mu$m-wall shell | |
| --- | --- | --- | --- | --- |
| | D$_2$ | N$_2$ | D$_2$ | N$_2$ |
| PAMS | $4.7 \times 10^{-15}$ | $1.6 \times 10^{-16}$ | 1.2 min | 34 min |
| Polyamic acid/PAMS | $8.4 \times 10^{-17}$ | – | 66 min | – |
| VDP polyimide | $2.0 \times 10^{-14*}$ | $8.5 \times 10^{-15*}$ | 17 s | 39 s |

*Data obtained using flat films.

for a 1-mm-outer-diam, 5-$\mu$m-wall shell would be 17 s for deuterium and 39 s for nitrogen. These very short values may explain why we were unable to measure time constants of actual shells.

4. Mechanical Properties and Behavior of Polyimide Shells

The elastic modulus and tensile strength of the polyimide shells must be known to define the necessary conditions to deliver DT-filled cryogenic targets: (1) the greater the elastic modulus, the greater the buckling pressure the target can withstand, and (2) the greater the tensile strength, the greater the burst pressure the target can endure. When combined with the permeation rate, these values determine the maximum rate at which the target can be filled and cooled for ICF cryogenic experiments.

Shells with a diameter between 800 and 900 $\mu$m and a wall thickness between 5 and 9 $\mu$m were repeatedly pressurized and depressurized using the protocol and equipment described previously. The shell's buckle- and burst-pressure differential was measured with an accuracy of ±5 psi (0.34 atm). The initial pressurization rate was 0.01 atm/s and the maximum pressure was 45 atm. The depressurizing rate was 50 atm/s. (The minimum pressurization rate was based on initial estimations for permeability and elastic modulus of polyimide.) All of the shells survived every test. The pressurizing rate was increased to 3.5 atm/s, the maximum that could be achieved, to minimize permeation that would decrease the pressure differential across the shell wall. Shells deposited using the plasma-assisted technique buckled at an overpressure of ~36 atm. The failure mechanism was atypical of polystyrene and plasma polymers: an indent developed in the shell and the shell did not catastrophically disintegrate (Fig. 71.22). These shells exhibit a greater fracture toughness than do existing ICF targets. The shells deposited by the thermionic-assisted technique were more durable than those deposited by the plasma-assisted technique and did not buckle or burst.

The maximum pressure rating of the test apparatus was increased to 105 atm; shells deposited using thermionic assistance were repeatedly tested at incrementally higher pressures. The 8-$\mu$m-wall polyimide shell survived the maximum pressurization rate of 3.5 atm/s to 105 atm. Using the calculated permeation rate for nitrogen through polyimide (measured above), the maximum pressure differential across the shell wall (the buckle pressure) was ~60 atm, and, using the standard expression for the crush pressure,

$$P_{\text{buckle}} = \frac{2E}{\sqrt{3(1-\nu^2)}}\left(\frac{w}{r}\right)^2,$$

where $E$ is the Young's modulus, $\nu$ is the Poisson ratio, $w$ is the wall thickness, and $r$ is the shell radius;[17] the modulus of the material was calculated to be ~15 GPa. For comparison, the



←— 845 $\mu$m —→

T1362

Figure 71.22

Plasma-assisted polyimide shell buckled at an external overpressure of ~36 atm. The shell did not brittle fracture, indicating a high fracture toughness.

largest reported literature value for the modulus of a solution-cast polyimide is 9.3 GPa. (A 1-mm-diam, 10-$\mu$m-thick shell would crush with an external overpressure of 44 atm.)

All attempts to burst the shells deposited by the thermionic-assisted technique were unsuccessful. Shells were gradually filled with nitrogen at a rate of ~4 atm/min to a final pressure of 110 atm and rapidly depressurized at the maximum rate possible (~50 atm/s). Assuming that negligible permeation occurred during the 2-s depressurizing cycle, the burst pressure was greater than 100 atm. Using this pressure value and the standard hoop stress equation, $P_{\mathrm{burst}} = 2T(w/r)$, the tensile strength $T$ was calculated to be greater than 300 MPa. For reference, the highest reported tensile strength for a solution-cast polyimide is 420 MPa.

The same polyimide shell was sputter coated with a 1-$\mu$m-thick aluminum layer to provide a permeation barrier layer, and the identical pressurization test was repeated. The shell neither buckled during pressurization nor burst during rapid depressurization. The calculated strength and modulus of polyimide shells are compiled in Table 71.VI.

5. Residual Stress Induced in Polyimide Films

As discussed previously, the imidizing cycle is the critical processing phase that affects the survivability and the resulting properties of the shells. The chemical changes that occur during the curing cycle have been described, and the effect these changes have on the mechanical properties of the film are now discussed.

As the temperature increases through the imidizing cycle, polyamic acid reacts (loses water) to form a polyimide. Unreacted monomers present in the film are sublimed, and the molecular weight and rigid structure of the polyimide increase. These mass, morphology, and structural changes alter the intrinsic stress in the polymer. If the polyamic acid was an unconstrained freestanding shell, the induced stress would be reduced by the shell shrinking or expanding to relieve the induced radial and hoop stresses. However, that stress-relief mechanism does not occur at lower temperatures where the PAMS mandrel possesses sufficient strength to resist these dimensional changes.

Below 110°C, the mandrel possesses significant material strength that constrains the polyamic acid. Above 110°C, the mandrel softens and the polyamic acid/polyimide can increasingly shrink or expand to relax the induced stress. Between 110°C and 180°C the $\alpha$-methylstyrene vapor pressure increases within the shell and, together with the slumping PAMS mandrel, produces a nonuniform burst pressure on the polyamic acid/polyimide wall. (All the shells heated at rates greater than 1°C/min through the 110°C to 180°C regime exploded. Depolymerization of a typical PAMS mandrel would produce an estimated burst pressure of 45 atm at 150°C in the absence of permeation.) Above 180°C the polyamic acid continues to imidize and the PAMS mandrel has a decreasing influence on the process. All these effects contribute at varying degrees to the instantaneous stress in the shell wall.

The magnitude of stress in the polyamic acid/polyimide composite film at the important processing temperatures (100, 140, 165, 220, and 300°C) was measured using a 14-$\mu$m polyamic acid film deposited on a silicon witness beam, as shown in Fig. 71.23. These data are corrected for the extrinsic thermal stress. (Flat films were used because no suitable technique was available to measure the stress that evolves in a shell.) Note: The data measured only the stresses that develop in polyimide during a specific cure cycle; additional stresses will exist in the polyimide shell because of the spherical geometry and the presence of the mandrel.

The intrinsic stress in the as-deposited film was ~15 MPa compressive. Heating the film to 100°C for 3 h induced a tensile stress. The maximum induced stress was 17 MPa at 165°C, where, coincidentally, the induced tensile stress offset the initial compressive stress. The tensile nature of the stress was expected as the film lost mass but was constrained at the interface by the substrate.

Table 71.VI:   Calculated strength and modulus of polyimide shells made by the two techniques.

| | Elastic Modulus (GPa) | Ultimate Tensile Strength (MPa) |
|---|---|---|
| Plasma-assisted polyimide | 5.5 | 95 |
| Thermionic-assisted polyimide | ~15 (minimum) | 300 (minimum) |
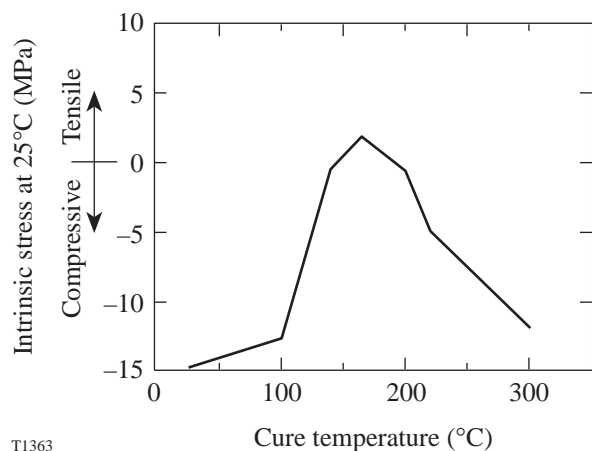
**Figure 71.23**
Temperature dependence of the intrinsic stress at 25°C in a polyamic acid/polyimide film.

As the temperature increased to 300°C, the compressive stress in the film returned to 14 MPa. The origin of this stress may be explained by steric considerations: as the molecular weight of the polyimide increased, the polymer chains became more rigid and the scale length of the polyimide increased. This repelling interference of the polyimide chains was constrained by the chains being intertwined and cross-linked, resulting in a compressive force. This behavior would be expected to increase the porosity (nanoscale) of the material and may also explain why the imidized material is more permeable than the polyamic acid.

The geometry of the shell creates an additional stress not present in an unconstrained film: the inner surface will be under greater compressive strain than will the outer surface, and the resulting stress will be in addition to the intrinsic stress measured above. The stress difference will be small for thin-walled, OMEGA-size shells, and, since the magnitude of the intrinsic stress is expected to be small, the induced residual stresses in the shell wall are not significant. Knowing how the intrinsic stress changes with temperature will be used to optimize the imidizing cycle to obtain thinner-walled shells.

By contrast, NIF targets are thick-walled shells, and it is possible that a sizable stress gradient will exist across the wall. When the shell is filled to its specified pressure (currently 360 atm), the maximum tensile stress will be at the inner surface. And, if a sizable residual stress is also present, the maximum pressure rating of the target will be reduced. These considerations make it important to know the magnitude of the induced stress. A desirable property of the polyimide shells observed here was the fracture toughness of the material; if the inner surface of a target experienced a localized highly strained region and a crack developed, the crack would help dissipate the stress, thereby avoiding catastrophic shell failure. This property may make transporting NIF cryogenic targets at room temperature more feasible.

**Summary**

A viable method for fabricating polyimide shells as potential targets for direct-drive ICF cryogenic experiments on OMEGA has been demonstrated. Shells with diameters ranging from 0.7 to 0.9 mm and wall thicknesses from 4 to 13 $\mu$m have been fabricated. Initial estimates of the elastic modulus, tensile strength, permeability, stress, composition, surface roughness, and burst/buckle pressures have been obtained. All of the effort discussed here has been devoted to obtaining polyimide shells and characterizing the resulting properties. No attempt has been made to optimize the processing conditions to improve the material properties. Importantly, no fundamental impediments were observed that would prevent polyimide shells being used as ICF targets. However, there are clearly many areas where the quality of the shell must be improved before the targets can be used for cryogenic experiments. That effort is the subject of future work.

The initially proposed mechanical-strength advantages of polyimide material have been experimentally substantiated: The shells are significantly stronger than existing polystyrene and plasma polymer shells. An initial concern about the low permeability of polyimide has been dispelled. In fact, the permeability is so high that future study is required to confirm that the permeability is an inherent material property and that the data are not distorted by unobserved interconnected porosity. Also, the impermeability of the shell at 20 K must be demonstrated.

REFERENCES

1. J. J. Sanchez and S. A. Letts, Fusion Technol. **31**, 491 (1997).

2. T. Takekoshi, in *Polyimides: Fundamentals and Applications,* edited by M. Ghosh and K. Mittal, Plastics Engineering, Vol. 36 (Marcel Dekker, New York, 1996), p. 7.

3. J. R. Salem *et al.*, J. Vac. Sci. Technol. A **4**, 369 (1986).

4. M. Iijima *et al.*, J. Vac. Sci. Jpn. **28**, 437 (1985).

5. S. A. Letts *et al.*, Fusion Technol. **28**, 1797 (1995).

6. S. A. Letts, D. W. Myers, and L. A. Witt, J. Vac. Sci. Technol. **19**, 739 (1981).

7. E. L. Alfonso, S.-H. Chen, M. D. Wittman, S. Papernov, and D. Harding, Polymer **38**, 1639 (1997).

8. B. McQuillan, presented at the ICF Target Fabrication Meeting, FY97 Mid-Year Review, San Diego, CA, 23–25 April 1997.

9. C. W. Hutchings and M. Grunze, Rev. Sci. Instrum. **66**, 3943 (1995).

10. Y. Takahashi *et al.*, Macromolecules **24**, 3543 (1991).

11. M. Bonino, R. Q. Gram, D. Harding, S. Noyes, J. Soures, and M. Wittman, presented at the Eleventh Target Fabrication Specialists' Meeting, Orcas Island, WA, 9–12 September 1996.

12. *Annual Book of ASTM Standards*, ASTM Designation: D 1434 - 82 (Reapproved 1992) (1994), Vol. 15.09, pp. 204–215.

13. G. G. Stoney, Proc. R. Soc. Lond. A **82**, 172 (1909).

14. J.-H. Jou *et al.*, J. Polym. Sci. Polym. Phys. Ed. **34**, 2239 (1996).

15. M. Langsam, in *Polyimides: Fundamentals and Applications*, edited by M. Ghosh and K. Mittal, Plastics Engineering, Vol. 36 (Marcel Dekker, New York, 1996), p. 697.

16. R. M. Ikeda *et al.*, J. Appl. Polym. Sci. **25**, 1391 (1980).

17. T. H. Hsu, *Structural Engineering & Applied Mechanics Data Handbook*, Volume 4: Shells (Gulf Publishing Company, Houston, 1991), p. 349.